

Half a Million Binary Stars identified from the low resolution spectra of LAMOST

YINGJIE JING,¹ TIAN-XIANG MAO,¹ JIE WANG,^{1,2,3} CHAO LIU,^{4,3,2} AND XIAODIAN CHEN^{5,3,2}

¹*National Astronomical Observatories, Chinese Academy of Sciences, Beijing, 100101, China*

²*Institute for Frontiers in Astronomy and Astrophysics, Beijing Normal University, Beijing 102206, China*

³*University of Chinese Academy of Sciences, 19 A Yuquan Rd, Shijingshan District, Beijing, 100049, China*

⁴*Key Laboratory of Space Astronomy and Technology, National Astronomical Observatories, Chinese Academy of Sciences, Beijing 100101, China*

⁵*CAS Key Laboratory of Optical Astronomy, National Astronomical Observatories, Chinese Academy of Sciences, Beijing 100101, China*

ABSTRACT

Binary stars are prevalent yet challenging to detect. We present a novel approach using convolutional neural networks (CNNs) to identify binary stars from low-resolution spectra obtained by the LAMOST survey. The CNN is trained on a dataset that distinguishes binaries from single main sequence stars based on their positions on the Hertzsprung-Russell diagram. Specifically, the training data labels stars with mass ratios between approximately 0.71 and 0.93 as intermediate mass ratio binaries, while excluding those beyond this range. The network achieves high accuracy with an area under the receiver operating characteristic curve of 0.949 on the test set. Its performance is further validated against known eclipsing binaries (97% detection rate) and binary stars identified by radial velocity variations (92% detection rate). Applying the trained CNN to a sample of one million main sequence stars from LAMOST DR10 and Gaia DR3 yields a catalog of 468,634 binary stars, which are mainly intermediate mass ratio binaries given the training data. This catalog includes 115 binary stars located beyond 10 kpc from the Sun and 128 cross-matched with known exoplanet hosts from the NASA Exoplanet Archive. This new catalog provides a valuable resource for future research on the properties, formation, and evolution of binary systems, particularly for statistically characterizing large populations.

Keywords: Main sequence stars(1000) — Binary stars(154) — Convolutional neural networks(1938)

1. INTRODUCTION

Binary and multiple star systems are ubiquitous, comprising roughly half of all stars. Understanding these systems is fundamental to various areas of astronomy. For instance, precise measurements of mass, radius, and luminosity are possible for stars in binary systems (e.g. Torres et al. 2010; Eker et al. 2018). Furthermore, binaries are crucial for testing theories of stellar formation and evolution, galactic archaeology, gravitational waves, and high-energy astrophysics (e.g. Duquennoy & Mayor 1991; Raghavan et al. 2010; Duchêne & Kraus 2013; Moe & Di Stefano 2017; Breivik et al. 2019; Tauris & van den

Heuvel 2023). Some binary systems even serve as valuable distance indicators (Kang et al. 2007; Pietrzyński et al. 2013). Therefore, the availability of a larger sample of binary systems is indispensable and advantageous for conducting comprehensive studies in the aforementioned fields.

Traditional methods for identifying binary stars include detecting variations in radial velocity (e.g. Pryor et al. 1988; Cote et al. 1994; Cote & Fischer 1996) or brightness (light curves) (e.g. Yan & Mateo 1994; Albrow et al. 2001; Milone et al. 2012). The Kepler mission, using light curve data, has been particularly successful in identifying thousands of eclipsing binaries (e.g., Kirk et al. 2016; Abdul-Masih et al. 2016). However, these methods often require multiple observations over time and are most effective for bright, close binaries with short orbital periods. Analyzing the color-magnitude diagram (CMD) provides another approach, as binaries tend to be brighter and redder than single

Corresponding author: Yingjie Jing
jjj@nao.cas.cn

Corresponding author: Jie Wang
jie.wang@nao.ac.cn

main-sequence stars of the same mass (e.g. Sollima et al. 2010; Milone et al. 2012; Li et al. 2013). Sophisticated statistical techniques applied to CMDs have improved the precision of this method (e.g. Hurley & Tout 1998; Naylor & Jeffries 2006; Sarro et al. 2014; Sheikhi et al. 2016; Li et al. 2017; Liu 2019; Li et al. 2020). Despite these advancements, the number of identified binaries remains limited.

Large spectroscopic surveys such as APOGEE (Holtzman et al. 2015), RAVE (Steinmetz et al. 2006), LAMOST (Cui et al. 2012; Zhao et al. 2012) offer new opportunities for binary star research. These surveys enable the identification of spectroscopic binaries (SBs) through Doppler shifts in their spectral lines (see review by Merle et al. 2020). The composite spectra of double-lined spectroscopic binaries (SB2s) provide additional clues. SBs cover a wide range of stellar masses and orbital periods (Sod 2004), and their detection is less affected by distance, making them well-suited for large-scale studies. Previous work using these spectroscopic surveys has resulted in binary star catalogs ranging in size from hundreds (RAVE, e.g. Matijević et al. 2010; Birko et al. 2019a) to thousands (APOGEE, e.g. Price-Whelan et al. 2018; El-Badry et al. 2018; Kounkel et al. 2021). Studies using low-resolution LAMOST spectra have identified hundreds of thousands of binaries (e.g., Liu et al. 2024b; Qian et al. 2019; Liu et al. 2024a). Zhang et al. (2022) find several thousand binary stars from LAMOST median resolution spectra. Similarly, Gaia data (Gilmore et al. 2012; Gaia Collaboration et al. 2016, 2023) have led to even larger catalogs, with over a million binaries identified using Gaia eDR3 (El-Badry et al. 2021).

Spectroscopic binaries exhibit distinctive spectral features that enable direct identification through analysis of their stellar spectra. While conventional methods often rely on fitting observed spectra to template spectra (e.g., El-Badry et al. 2018; Traven et al. 2020), neural networks offer a more powerful and efficient alternative (see reviews by Lecun et al. 2015; Goodfellow et al. 2016). Neural networks excel at complex tasks by learning intricate patterns from data, eliminating the need for manual feature engineering. This data-driven approach is particularly well-suited for binary star classification. In this work, we leverage the large volume of low-resolution stellar spectra from the LAMOST survey (Cui et al. 2012; Zhao et al. 2012) and employ convolutional neural networks (CNNs) (e.g., LeCun et al. 1990; Krizhevsky et al. 2012) to identify binary stars. CNNs and other artificial neural networks have been successfully applied to various astronomical problems (e.g., Ting et al. 2018; Davies et al. 2019; Pearson et al. 2019), and we expect

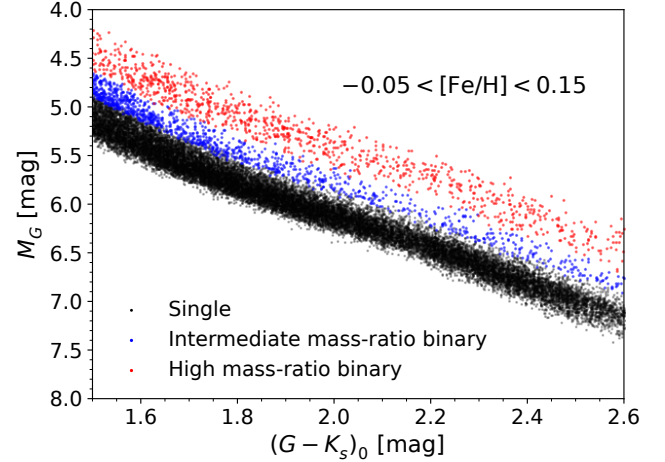


Figure 1. Color-magnitude diagram for stars with $-0.05 < [\text{Fe}/\text{H}] < 0.15$ from the train sample. The black, blue, and red points represent identified single main sequence, intermediate, and high mass-ratio binary stars, respectively. The single stars and intermediate mass ratio binaries are selected as training sample. The G-band absolute magnitude (M_G) is plotted against the dereddened color index $(G - K_s)_0$.

them to be effective in extracting relevant information from spectral features for binary star detection.

The paper is organized as follows: Section 2 details the dataset along with the network model. Section 3 reviews our model’s performance and offers a catalog of main sequence binary stars. Section 4 summarizes the outcomes of our study.

2. DATA AND METHODS

2.1. Dataset

In order to train the neural network, a larger number of binary and single star spectra are needed. We utilized the star sample from the Liu (2019) which selected a solar neighborhood stars sample and identified the single and binary stars based on the fact that binary sequence is located above the single main sequence in Hertzsprung-Russell (HR) diagram. For illustrative purposes, we present a color-magnitude diagram (CMD) for stars within a $[\text{Fe}/\text{H}]$ range ($-0.05 < [\text{Fe}/\text{H}] < 0.15$) from this sample in Figure 1. Here, CMD is the dereddened color index $(G - K_s)_0$ compared to the absolute magnitude of the G band M_G . Unresolved binary stars exhibit a brighter absolute magnitude compared to single stars. With a larger shift $\Delta M_G = M_G - M_{G,\text{single}}$, the probability that the star is a binary increases, as does the likelihood of a high mass ratio if it is binary (see also Figure 9 in Liu (2019)).

Specifically, we labeled stars with ΔM_G values between -0.25 and 0.25 as single stars (represented by black points in Figure 1). Stars with ΔM_G values

between -0.5 and -0.25 (shown in blue points) were labeled as binaries (corresponding to an intermediate mass ratios between approximately 0.71 and 0.93). The threshold of $\Delta M_G = -0.25$ was chosen to ensure the purity of the binary sample, accounting for magnitude uncertainties. High-mass-ratio binaries ($\Delta M_G < -0.5$, red points) were excluded from our training set because their spectra are very similar to single star spectra, making spectral-based discrimination challenging. Following these selection criteria, our final training sample consisted of 68,299 single stars and 3,818 binary stars. These stars were subsequently divided into training, validation, and test sets, as described in the following subsection.

We constructed our initial stellar sample by cross-matching stars from LAMOST DR10 low-resolution A, F, G and K stars catalog (<https://www.lamost.org/dr10/>), Gaia DR3 (Gaia Collaboration et al. 2016, 2023), and 2MASS (Skrutskie et al. 2006) following the procedure outlined in Liu (2019). This initial sample includes about 7 million spectra. The LAMOST low-resolution spectra span a wavelength range of 3700 to 9000 Å, with a resolution of $R \approx 1800$ (Cui et al. 2012; Luo et al. 2012).

The train sample from Liu (2019) satisfies the following selection criteria:

1. $3800 < T_{\text{eff}} < 6500$ K;
2. $\log g > 4$;
3. $1.5 < (G - K_s)_0 < 2.6$;
4. signal-to-noise ratio at g band of LAMOST spectra is larger than 20;
5. $\varpi > 3$ so that most of the stars are located within ~ 300 pc (excluded in this work);
6. G-band absolute magnitude $M_G > 4\text{mag}$ (excluded in this work).

As our network relies exclusively on spectra for input, we have excluded selection criteria 5 and 6. Consequently, our final main sequence stars sample comprises 1,258,912 spectra associated with 971,805 stars, many of which have been observed multiple times.

2.2. Spectra Data Preprocessing

Before generating the training set, various data preprocessing steps are taken to enhance the network's performance. Initially, data cleaning is applied to eliminate spectra with excessively masked data points. Subsequently, each flux spectrum is interpolated onto a new

wavelength grid and normalized by dividing by the corresponding smoothed flux $f_s(\lambda)$ (Ho et al. 2017). The definition of smoothed flux $f_s(\lambda)$ is

$$f_s(\lambda) = \frac{\sum_i (f_i w_i(\lambda))}{\sum_i (w_i(\lambda))}, \quad (1)$$

where f_i is the flux at λ_i and the weight $w_i(\lambda)$ is a Gaussian function

$$w_i(\lambda) = e^{-\frac{(\lambda - \lambda_i)^2}{\sigma^2}}. \quad (2)$$

The σ is set to 35 nm to eliminate large-scale variations. We then use the entire spectrum, with wavelengths ranging from 3700 to 9000 Å, as input to the network.

We randomly divide the aforementioned data set in an 80%, 10%, 10% split to form the training, validation, and test sets. In particular, since the proportion of binary stars to single stars is approximately 1 : 18 in our training set, this classification poses an imbalance issue. The impact of class imbalance on classification performance is both harmful and intricate (Buda et al. 2017). To mitigate this impact, we adopt the method described in Buda et al. (2017) to oversample binary stars to match the number of single stars by repeatedly sampling within the training set.

2.3. Deep learning model

The basic structure of CNNs is named the convolutional layer, which is defined as

$$\mathbf{x}_n^l = a \left(\sum_k \mathbf{W}_n^l \otimes \mathbf{x}_{n-1}^k + \mathbf{b}_n^l \right). \quad (3)$$

Here, \otimes indicates the convolution operation, \mathbf{W}_n^l denotes the trainable convolutional kernels of layer n , l indicates the l -th kernel in this layer and k indicates the output corresponding to the k -th convolutional kernel of the previous layer. Since we hope to classify the binary stars from the spectra data, the convolution operation \otimes means 1-D convolution in this work.

The architecture of our network includes a basic residual learning block (refer to Figure 2 in He et al. (2015)) followed by two fully connected layers. To mitigate the risk of overfitting due to the limited number of binary star samples, we integrate dropout layers (Srivastava et al. 2014) within the fully connected layers at a rate of 0.5 and employ early stopping during training. We utilize the cross-entropy loss function and set the learning rate as $1e^{-4}$. For each spectrum, the trained network estimates the probability p_b of it being a binary star, with the value of p_b lying between 0 and 1.

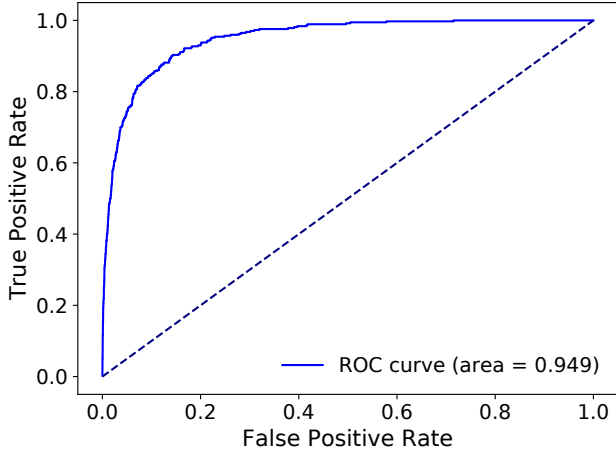


Figure 2. Receiver Operating Characteristic (ROC) curve for the test set. The solid blue line represents the performance of the trained CNN model, while the dashed orange line indicates the ROC curve for random selection. The area under the curve (AUC) for the model is 0.949, demonstrating significantly better performance than random classification.

3. RESULTS

In this section, we will assess the network’s performance using the test set and known binary stars samples from previous studies. These binary star samples include eclipsing binaries and binary stars identified from variations in radial velocity. We then apply the network to the entire sample.

3.1. Test set

The receiver operating characteristic (ROC) curve is frequently utilized to assess the efficacy of a binary classification system. A larger area under the ROC curve indicates superior performance by the classifier. The ROC curve is a graph plotting the true positive rate (TPR) versus the false positive rate (FPR) at various thresholds. In Figure 2, the ROC curve for the test set is represented by a solid line. For comparison, a dashed line denotes the ROC curve for a random sample, which has an area of 0.5. The ROC curve of the test set is significantly better than that of random selection, covering a larger area (0.949).

We present the probability density distribution function (PDF) of p_b for both single and binary stars in the test set in Figure 3. The majority of single stars (95.5%) exhibit a p_b less than 0.2, while most binary stars (73%) demonstrate a p_b greater than 0.8. This indicates that the network performs well in classifying star spectra. To ensure the binary stars identified by the network are as accurate as possible, we estimate the precision, which is dependent on the threshold cut-off of p_b , denoted as p_{th} , and the binary-to-single star ratio r in the input sample.

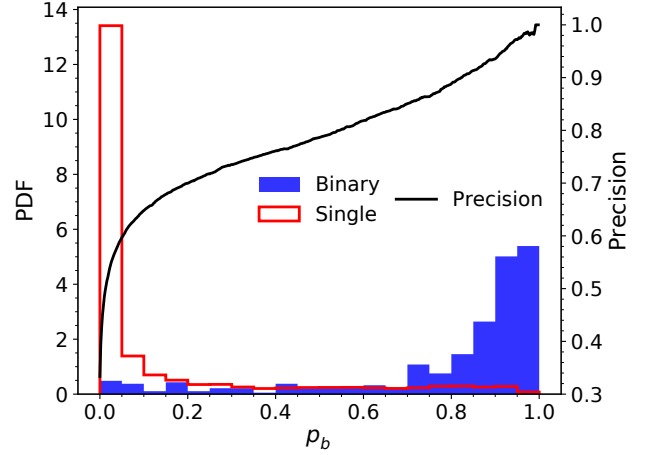


Figure 3. Probability density function (PDF) of the predicted probabilities (p_b) for binary (blue region) and single (red line) stars in the test set. The black line shows the precision as a function of the adopted probability cut-off threshold, assuming a binary-to-single star ratio of 1:2.

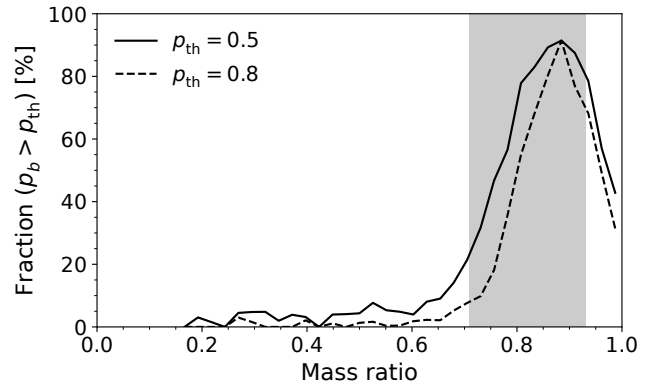


Figure 4. The fraction of binary stars as a function of mass ratio for different p_{th} values. The shaded area denotes the regions of intermediate-mass-ratio binaries (corresponding to mass ratios between approximately 0.71 and 0.93) which is included in the train sample.

The precision is defined as

$$\text{Precision} = \frac{N_{TP}}{N_{TP} + N_{FP} \times N_b/N_s/r}, \quad (4)$$

where N_b and N_s are the number of binary and single stars in our test set, respectively, and N_{TP} and N_{FP} represent the number of true positive (correctly identified binary) and false positive (single star misclassified as binary) classifications with $p_b > p_{th}$, respectively. By fixing the binary-to-single ratio at 1 : 2, we illustrate the precision as a function of p_{th} in the black curve of Figure 3. Our results illustrate that the precision reaches 0.79 (0.89) when p_{th} is set to 0.5 (0.8).

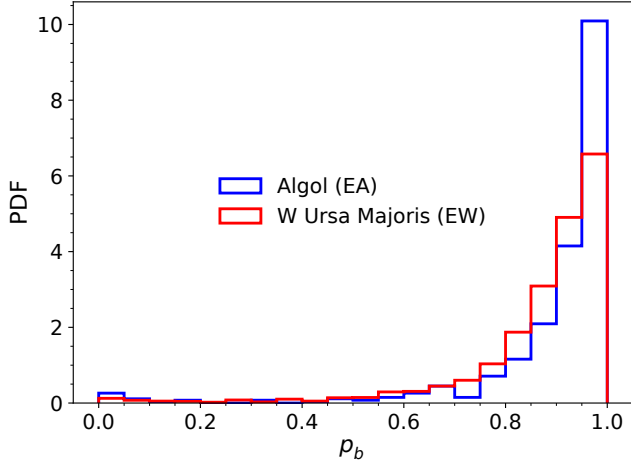


Figure 5. Probability density function (PDF) of the predicted binary probabilities (p_b) for eclipsing binary stars. The blue solid line corresponds to Algol-type (EA) binaries, while the red solid line corresponds to W Ursa Majoris-type (EW) binaries, demonstrating a high detection rate of 96.45% for EA and 96.40% for EW binaries.

It is also worth to investigate how the network’s sensitivity changes with different mass ratios. Figure 4 displays the fraction of stars classified as binaries as a function of their mass ratio driven by Liu (2019), for different probability thresholds (p_{th}). The stars shown in this figure are from the test set and high-mass-ratio stars from Liu (2019). A trend influenced by the training data is evident. The binary fraction is highest for mass ratios around 0.71-0.93, which is indicated by the shaded region and corresponds to the intermediate-mass-ratio binaries used in the training process. The figure shows a decrease in the binary fraction as mass ratios close to 1. This is partially a result of the exclusion of high-mass-ratio binaries ($\Delta M_G < -0.5$) from the training data, which is due to the intrinsic similarity of their spectra to those of single stars. For low mass ratios, the sensitivity decreases significantly. This is likely due to the training data using specific cuts on ΔM_G to distinguish between single stars and intermediate-mass-ratio binaries. While we expect that a more comprehensive training sample might improve the detection rate for lower mass ratio, the detection of highest mass ratio binaries may remain difficult due to the limitations in spectrally distinguishing them from single stars. The overall fraction of classified binaries is also shown to be lower for curves with higher p_{th} values across all mass ratios.

3.2. Comparison with other methods

In this subsection, we evaluate our network by comparing it with a sample of eclipsing binary stars and a sample based on radial velocity variations.

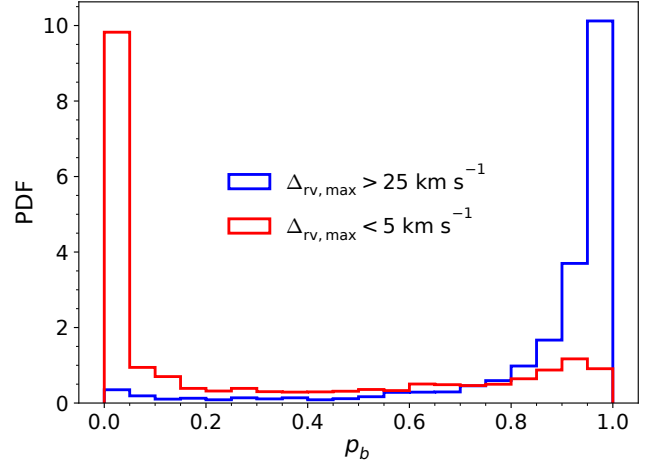


Figure 6. Probability density function (PDF) of the predicted binary probabilities (p_b) for stars observed multiple times in the LAMOST survey. The blue line indicates potential binary stars (with $\Delta_{rv,max} > 25 \text{ km s}^{-1}$), while the red dashed line indicates likely single stars (with $\Delta_{rv,max} < 5 \text{ km s}^{-1}$).

Eclipsing binaries (EBs) are identified by the periodic variations in their apparent magnitude, known as the light curve, which are due to geometric attributes rather than spectral characteristics. Therefore, they serve as an excellent independent validation verification for our network. In this work, we used a sample of Algol (EA) type and W Ursa Majoris (EW) type eclipsing binary stars from the Chen et al. (2020), which detected 350,000 eclipsing binaries from Zwicky Transient Facility. We cross-matched their sample with our main sequence stars sample, obtaining 535 EA and 2,724 EW common eclipsing binary stars. The blue and red solid lines in Figure 5 depict the probability density function of p_b for EA and EW binary stars, respectively. By setting p_{th} to 0.5, 96.45% of EA and 96.40% of EW eclipsing binary stars are correctly identified as binary stars, demonstrating the high performance of our network.

We subsequently compared our network’s predictions with results derived from variations in radial velocity. In a binary star system, both stars revolve around a shared center of mass. Consequently, unless the orbital plane is perpendicular to our line of sight, the radial velocity observed from the system’s spectrum will vary over time. In contrast, a single star’s radial velocity will remain relatively constant. This distinction is utilized to identify binary stars (e.g. Price-Whelan et al. 2018; Birkel et al. 2019b; Qian et al. 2019). The LAMOST survey has observed numerous stars on multiple occasions. For stars with at least two observations and a maximum radial velocity difference, $\Delta_{rv,max} > 25 \text{ km s}^{-1}$, we classify them as potential binary stars. Conversely, stars observed

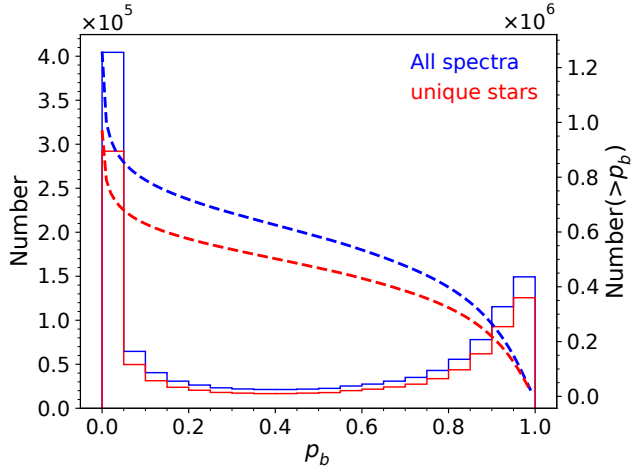


Figure 7. The distribution of p_b provided by the network for all spectra (blue) and individual stars (red) within the main sequence star sample. The solid curves represent the number distribution of p_b , while the dashed lines indicate the count of spectra (or individual stars) with as a function of the p_{th} . For individual stars, p_b corresponds to the highest value in cases of multiple observations.

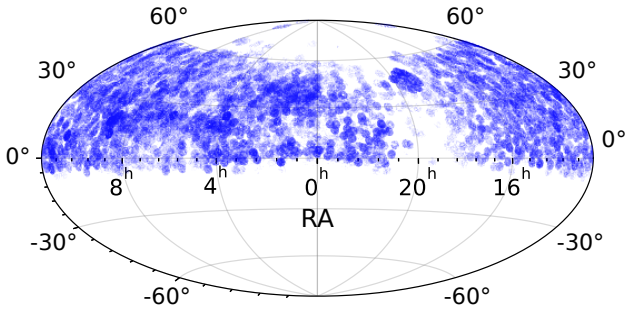


Figure 8. Distribution of binary stars in the Right Ascension (RA) and Declination (Dec) plane.

four or more times with $\Delta_{rv,max} < 5 \text{ km s}^{-1}$ are classified as likely single stars. We applied our network to both groups and plotted their probability density functions (PDFs) of p_b in Figure 6, where the black solid and cyan dashed lines represent the PDFs for possible binary and single stars, respectively. With a threshold probability p_{th} of 0.5, our network’s prediction aligns with radial velocity variations for 92.8% of binary stars and 68.8% of single stars. We notice that the alignment for single stars is not as high as for binary stars, possibly because some stars in long-period binary systems exhibit minimal radial velocity changes, which LAMOST has not detected.

3.3. Main sequence binary stars catalogue

Following the evaluation of the network’s performance, we applied it to our sample main sequence star

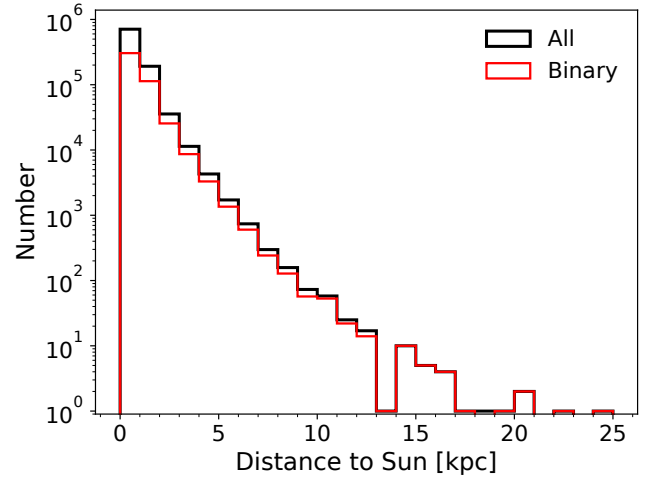


Figure 9. Distribution of distances to the Sun for all stars (black) and binary stars (red). The histogram reveals that binary stars are found at a range of distances, with 115 binary stars situated beyond 10 kpc.

sample. We selected spectra with $p_b > 0.5$ for incorporation into our primary catalog of binary stars on the main sequence (Table 1). The catalog contains 468,634 stars¹, with 323,909 of them having $p_b > 0.8$. The threshold selection is a compromise between accuracy and purity. Although we used a threshold of $p_{th} = 0.5$ in this study, our published binary star catalog includes the p_b value for each star to allow custom threshold selection based on specific requirements.

Qian et al. (2019) detected binary stars from LAMOST using a method based on variations in radial velocity from multiple observations of stellar spectra. Our network necessitates just a single observation of star spectra, but it is restricted to main sequence stars due to the limitations in the training dataset. They identified 256,000 spectroscopic binary or variable stars, slightly fewer than our findings. Our catalog surpasses prior spectroscopic binary star studies in size. For instance, Jack (2019) identified 34,691 spectroscopic binary stars by comparing Gaia DR2 with other radial velocity catalogs, while Birko et al. (2019b) discovered 27,716 SB1 from 450,646 stars with multiple radial velocity measurements in the RAVE and Gaia DR2 surveys. Additionally, Price-Whelan et al. (2018) found 4,898 SB1 amongst 96,231 red giant stars observed in the APOGEE survey.

We subsequently analyze the catalog’s characteristics. Figure 7 illustrates the p_b distribution, with blue and red solid lines representing all spectra and stars, respec-

¹ The training samples are included in this final binary stars catalog.

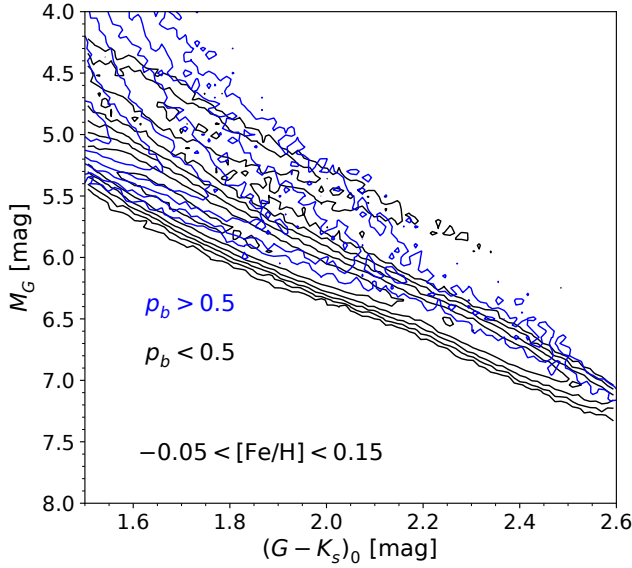


Figure 10. Number density contour plot in the color-magnitude diagram the stars with $-0.05 < [\text{Fe}/\text{H}] < 0.15$. Stars with $p_b < 0.5$ are shown in black contours, while those with $p_b > 0.5$ are highlighted in blue.

tively. For stars with multiple observational spectra, the p_b value corresponds to the maximum value. The majority of the spectra (or unique stars) have p_b values near zero or one, predicting as either single or binary star, without ambiguity. This shows a clear distinction in the binary status of the stars based on their p_b values, making the classification straightforward. The dashed lines depict the number of spectra (or stars) as a function of threshold p_{th} , indicating the count of those with p_b exceeding p_{th} . As p_{th} increases, the number decreases, yet the *Precision* (see Figure 3) of binaries improves.

Figure 8 illustrates the distribution of binary spectra ($p_{\text{th}} = 0.5$) within the RA-DEC plane. This distribution closely resembles the overall spectra distribution (not depicted). In Figure 9, we present the target distances from the Sun for total and binary stars, utilizing distances from Bailer-Jones et al. (2021). Our analysis reveals that the range of distances stretches up to roughly 19 kpc, with a median distance of about 0.7 kpc for binary stars. There are 115 binary stars situated at distances greater than 10 kpc from the Sun.

As the training sample differentiates single stars and binary stars in the color-magnitude diagram (CMD), it is valuable to examine the result from the network in the CMD. We plot single stars (chosen by $p_b < 0.5$) and binary stars (chosen by $p_b > 0.5$) within $-0.05 < [\text{Fe}/\text{H}] < 0.15$ on the CMD in Figure 10. The black and blue curves show the number density contour for single stars (chosen by $p_b < 0.5$) and binary stars, respectively.

Consistent with our expectations and similar to Figure 1, the predicted binary stars appear above the single stars' main sequence in the CMD, even though they lack a clear boundary. We also observed a small fraction of stars with $p_b < 0.5$ situated above binary stars. These stars are most likely binary stars with a high mass ratio (indicated by red points in Figure 1). Since their spectra resemble that of single stars, they were excluded from the training dataset and consequently not identified by the network, which is as anticipated. Nevertheless, this does not affect the accuracy of our binary star catalog.

3.4. Planets in binary stars system

Previous studies have demonstrated the existence of planets orbiting binary star systems (e.g. Desidera & Barbieri 2007; Mugrauer & Neuhäuser 2009), sparking significant interest in understanding planet formation and evolution within these dynamically complex environments (e.g. Thebault & Haghighipour 2015). We cross-matched our catalog of binary stars with the NASA Exoplanet Archive (NASA Exoplanet Archive 2024)²³. This yielded 128 binary star systems hosting confirmed exoplanets (Table 2). Remarkably, 114 of these systems were not previously identified as binary stars in the Exoplanet Archive, highlighting the contribution of our catalog. The catalog proves useful for future studies exploring the properties and formation of planets in binary star systems. These systems represent a diverse range of binary configurations and planetary architectures. Further analysis of this sample could shed light on the influence of stellar multiplicity on planet formation and evolution.

4. CONCLUSIONS AND DISCUSSIONS

In this study, we employed a convolutional neural network (CNN) to identify binary stars using low-resolution spectra from the LAMOST survey. Our CNN was trained on a dataset of 68,299 single stars and 3,818 intermediate mass-ratio binaries (between approximately 0.71 and 0.93) selected from Liu (2019), based on their distinct locations in the Hertzsprung-Russell diagram.

The performance of our network was rigorously evaluated using several methods. The area under the receiver operating characteristic curve (ROC) on a held-out test set reached 0.949, demonstrating a strong ability to differentiate between single and binary stars. Furthermore, our network achieved a high detection rate of approximately 96% when validated against a sample of known

² Accessed on 2024-09-24 at 02:31, returning 5759 rows.

³ <https://exoplanetarchive.ipac.caltech.edu/cgi-bin/TblView/nph-tblView?app=ExoTbls&config=PSCompPars>

Table 1. Main Sequence Binary Star Candidates

LAMOST-DR10-obsid	Gaia-DR3-source_id	RA (<i>hms</i>)	DEC (<i>dms</i>)	p_b	snrg
1411021	167617837532848128	03:59:05.55	+30:37:10.4	0.971	30.180000
1415160	167552897627512704	03:57:18.77	+29:48:32.3	0.941	36.910000
1415164	167551145280831232	03:58:10.41	+29:49:59.4	0.981	25.450001
1415222	167507130456235520	03:59:30.18	+29:50:41.7	0.889	34.400002
1415226	167106564626111744	03:58:33.72	+29:22:49.9	0.912	28.770000
...

Note: Full catalog available in the online journal and via DOI: [10.57760/sciencedb.15844](https://doi.org/10.57760/sciencedb.15844).

Table 2. Main Sequence Binary Star Candidates Hosting Exoplanets

hostname	LAMOST-DR10-obsid	Gaia-DR3-source_id	RA (<i>hms</i>)	DEC (<i>dms</i>)	p_b
Kepler-971	243016079	2103712163117363200	18:56:22.73	+41:10:58.0	0.895
Kepler-743	247607014	2077994272606400512	19:42:17.80	+42:48:23.2	0.756
Kepler-478	247616169	2128256492468364160	19:29:56.86	+46:11:46.4	0.704
Kepler-1332	247710091	2126102411750601088	19:24:06.86	+43:54:49.2	0.864
Kepler-1583	249201170	2130695518492411904	19:05:32.86	+47:01:00.0	0.960
...

Note: Full catalog available in the online journal and via DOI: [10.57760/sciencedb.15844](https://doi.org/10.57760/sciencedb.15844).

eclipsing binaries. Comparison with radial velocity variations from multi-epoch LAMOST observations showed a 92.8% agreement for binary stars and 68.8% for single stars. The lower agreement for single stars might be attributed to undetected long-period binaries exhibiting minimal radial velocity changes within the LAMOST observation baseline.

Applying our trained CNN to the selected main sequence sample of 971,805 stars from LAMOST yielded a catalog of 468,634 binary stars, which are mainly intermediate mass ratio binaries given the training data. The threshold of $p_b > 0.5$ for inclusion in the catalog represents a balance between maximizing the number of identified binaries and maintaining a high precision. However, the full catalog includes the p_b value for each star, allowing users to apply custom thresholds based on their specific requirements. The catalog spans a distance range up to ~ 19 kpc, with a median distance of ~ 0.7 kpc for binary stars, and includes 115 binaries located beyond 10 kpc. Interestingly, we also identified 128 binary systems hosting confirmed exoplanets by cross-matching our catalog with the NASA Exoplanet Archive.

A key advantage of our method is its ability to identify binary candidates using single-epoch spectra, unlike traditional radial velocity methods that require multiple observations. This makes our approach particularly valuable for large spectroscopic surveys like LAMOST. However, it is important to acknowledge limitations.

Our training sample focused solely on main sequence stars, potentially limiting the applicability of the CNN to other stellar types. Furthermore, potential biases in the training data may affect the network’s performance. Future work will focus on expanding the training dataset to include a wider range of stellar types and exploring alternative methods for training data selection to mitigate potential biases.

This large catalog of binary star candidates provides a valuable resource for future research on the formation, evolution, and statistical properties of binary systems, particularly for studies requiring large sample sizes. The catalog, along with individual values p_b , is available at <https://doi.org/10.57760/sciencedb.15844>.

ACKNOWLEDGMENTS

We would like to thank the referee for the constructive suggestions and comments. This work was supported by the China National Key Program for Science and Technology Research and Development of China (2022YFA1602901, 2023YFA1608204), the National Natural Science Foundation of China (Nos. 11988101, 11873051, 12125302, 12041305, 12173016, 12203065), the CAS Project for Young Scientists in Basic Research grant (No. YSBR-062), and the K.C. Wong Education Foundation, and the science research grants from the China Manned Space Project. We acknowledge the CSST research grants from the China Manned

Space Project. Y.J. acknowledges support from the Cultivation Project for FAST Scientific Payoff and Research Achievement of CAMS-CAS. JW acknowledges the hospitality of the International Centre of Supernovae (ICE-SUN), Yunnan Key Laboratory at Yunnan Observatories Chinese Academy of Sciences when we drafted this paper.

Guoshoujing Telescope (the Large Sky Area Multi-Object Fiber Spectroscopic Telescope LAMOST) is a National Major Scientific Project built by the Chinese Academy of Sciences. Funding for the project has been provided by the National Development and Reform Commission. LAMOST is operated and managed by the National Astronomical Observatories, Chinese Academy of Sciences.

This work has made use of data from the European Space Agency (ESA) mission *Gaia* (<https://www.cosmos.esa.int/gaia>), processed by the *Gaia* Data Processing and Analysis Consortium (DPAC, <https://www.cosmos.esa.int/web/gaia/dpac/consortium>). Funding for the DPAC has been provided by national institutions, in particular the institutions participating in the *Gaia* Multilateral Agreement.

This publication makes use of data products from the Two Micron All Sky Survey, which is a joint project of the University of Massachusetts and the Infrared Processing and Analysis Center/California Institute of Technology, funded by the National Aeronautics and Space Administration and the National Science Foundation.

REFERENCES

- 2004, Astronomical Society of the Pacific Conference Series, Vol. 318, Spectroscopically and Spatially Resolving the Components of the Close Binary Stars
- Abdul-Masih, M., Prša, A., Conroy, K., et al. 2016, *AJ*, 151, 101, doi: [10.3847/0004-6256/151/4/101](https://doi.org/10.3847/0004-6256/151/4/101)
- Albrow, M. D., Gilliland, R. L., Brown, T. M., et al. 2001, *The Astrophysical Journal*, 559, 1060–1081, doi: [10.1086/322353](https://doi.org/10.1086/322353)
- Bailer-Jones, C. A. L., Rybizki, J., Fouesneau, M., Demleitner, M., & Andrae, R. 2021, *AJ*, 161, 147, doi: [10.3847/1538-3881/abd806](https://doi.org/10.3847/1538-3881/abd806)
- Birko, D., Zwitter, T., Grebel, E. K., et al. 2019a, *AJ*, 158, 155, doi: [10.3847/1538-3881/ab3cc1](https://doi.org/10.3847/1538-3881/ab3cc1)
- . 2019b, arXiv e-prints, arXiv:1906.11486. <https://arxiv.org/abs/1906.11486>
- Breivik, K., Price-Whelan, A. M., D’Orazio, D. J., et al. 2019, Stellar multiplicity: an interdisciplinary nexus. <https://arxiv.org/abs/1903.05094v1>
- Buda, M., Maki, A., & Mazurowski, M. A. 2017, arXiv e-prints. <https://arxiv.org/abs/1710.05381>
- Chen, X., Wang, S., Deng, L., et al. 2020, *ApJS*, 249, 18, doi: [10.3847/1538-4365/ab9cae](https://doi.org/10.3847/1538-4365/ab9cae)
- Cote, P., & Fischer, P. 1996, *The Astronomical Journal*, 112, 565, doi: [10.1086/118034](https://doi.org/10.1086/118034)
- Cote, P., Welch, D. L., Fischer, P., et al. 1994, *The Astrophysical Journal Supplement Series*, 90, 83, doi: [10.1086/191858](https://doi.org/10.1086/191858)
- Cui, X.-Q., Zhao, Y.-H., Chu, Y.-Q., et al. 2012, *Research in Astronomy and Astrophysics*, 12, 1197, doi: [10.1088/1674-4527/12/9/003](https://doi.org/10.1088/1674-4527/12/9/003)
- Davies, A., Serjeant, S., & Bromley, J. M. 2019, *MNRAS*, 487, 5263, doi: [10.1093/mnras/stz1288](https://doi.org/10.1093/mnras/stz1288)
- Desidera, S., & Barbieri, M. 2007, *A&A*, 462, 345, doi: [10.1051/0004-6361:20066319](https://doi.org/10.1051/0004-6361:20066319)
- Duchêne, G., & Kraus, A. 2013, *Annual Review of Astronomy and Astrophysics*, 51, 269–310, doi: [10.1146/annurev-astro-081710-102602](https://doi.org/10.1146/annurev-astro-081710-102602)
- Duquennoy, A., & Mayor, M. 1991, *A&A*, 500, 337
- Eker, Z., Bakış, V., Bilir, S., et al. 2018, *Monthly Notices of the Royal Astronomical Society*, 479, 5491–5511, doi: [10.1093/mnras/sty1834](https://doi.org/10.1093/mnras/sty1834)
- El-Badry, K., Rix, H.-W., & Heintz, T. M. 2021, *MNRAS*, doi: [10.1093/mnras/stab323](https://doi.org/10.1093/mnras/stab323)
- El-Badry, K., Ting, Y.-S., Rix, H.-W., et al. 2018, *MNRAS*, 476, 528, doi: [10.1093/mnras/sty240](https://doi.org/10.1093/mnras/sty240)
- Gaia Collaboration, Prusti, T., de Bruijne, J. H. J., et al. 2016, *A&A*, 595, A1, doi: [10.1051/0004-6361/201629272](https://doi.org/10.1051/0004-6361/201629272)
- Gaia Collaboration, Vallenari, A., Brown, A. G. A., et al. 2023, *A&A*, 674, A1, doi: [10.1051/0004-6361/202243940](https://doi.org/10.1051/0004-6361/202243940)
- Gilmore, G., Randich, S., Asplund, M., et al. 2012, *The Messenger*, 147, 25
- Goodfellow, I., Bengio, Y., & Courville, A. 2016, *Deep Learning* (MIT Press)
- He, K., Zhang, X., Ren, S., & Sun, J. 2015, arXiv e-prints. <https://arxiv.org/abs/1512.03385>
- Ho, A. Y. Q., Ness, M. K., Hogg, D. W., et al. 2017, *ApJ*, 836, 5, doi: [10.3847/1538-4357/836/1/5](https://doi.org/10.3847/1538-4357/836/1/5)
- Holtzman, J. A., Shetrone, M., Johnson, J. A., et al. 2015, *The Astronomical Journal*, 150, 148, doi: [10.1088/0004-6256/150/5/148](https://doi.org/10.1088/0004-6256/150/5/148)
- Hurley, J., & Tout, C. A. 1998, *Monthly Notices of the Royal Astronomical Society*, 300, 977–980, doi: [10.1046/j.1365-8711.1998.01981.x](https://doi.org/10.1046/j.1365-8711.1998.01981.x)
- Jack, D. 2019, *Astronomische Nachrichten*, 340, 386, doi: [10.1002/asna.201913496](https://doi.org/10.1002/asna.201913496)

- Kang, Y. W., Hong, K. S., & Lee, J. 2007, in *Astronomical Society of the Pacific Conference Series*, Vol. 362, The Seventh Pacific Rim Conference on Stellar Astrophysics, ed. Y. W. Kang, H. W. Lee, K. C. Leung, & K. S. Cheng, 19
- Kirk, B., Conroy, K., Prša, A., et al. 2016, *AJ*, 151, 68, doi: [10.3847/0004-6256/151/3/68](https://doi.org/10.3847/0004-6256/151/3/68)
- Kounkel, M., Covey, K. R., Stassun, K. G., et al. 2021, *AJ*, 162, 184, doi: [10.3847/1538-3881/ac1798](https://doi.org/10.3847/1538-3881/ac1798)
- Krizhevsky, A., Sutskever, I., & Hinton, G. E. 2012, in *Advances in neural information processing systems*, 1097–1105
- Lecun, Y., Bengio, Y., & Hinton, G. 2015, *Nature*, 521, 436, doi: [10.1038/nature14539](https://doi.org/10.1038/nature14539)
- LeCun, Y., Boser, B. E., Denker, J. S., et al. 1990, in *Advances in neural information processing systems*, 396–404
- Li, C., de Grijs, R., & Deng, L. 2013, *Monthly Notices of the Royal Astronomical Society*, 436, 1497–1512, doi: [10.1093/mnras/stt1669](https://doi.org/10.1093/mnras/stt1669)
- Li, L., Shao, Z., Li, Z.-Z., et al. 2020, *The Astrophysical Journal*, 901, 49, doi: [10.3847/1538-4357/abaef3](https://doi.org/10.3847/1538-4357/abaef3)
- Li, Z.-M., Mao, C.-Y., Luo, Q.-P., et al. 2017, *Research in Astronomy and Astrophysics*, 17, 071, doi: [10.1088/1674-4527/17/7/71](https://doi.org/10.1088/1674-4527/17/7/71)
- Liu, C. 2019, *MNRAS*, 490, 550, doi: [10.1093/mnras/stz2274](https://doi.org/10.1093/mnras/stz2274)
- Liu, H.-B., Gu, W.-M., Zhang, Z.-X., et al. 2024a, *ApJ*, 969, 114, doi: [10.3847/1538-4357/ad4c6f](https://doi.org/10.3847/1538-4357/ad4c6f)
- Liu, J., Zhang, B., Wu, J., & Ting, Y.-S. 2024b, *arXiv e-prints*, arXiv:2410.07637, doi: [10.48550/arXiv.2410.07637](https://doi.org/10.48550/arXiv.2410.07637)
- Luo, A. L., Zhang, H.-T., Zhao, Y.-H., et al. 2012, *Research in Astronomy and Astrophysics*, 12, 1243, doi: [10.1088/1674-4527/12/9/004](https://doi.org/10.1088/1674-4527/12/9/004)
- Matijević, G., Zwitter, T., Munari, U., et al. 2010, *AJ*, 140, 184, doi: [10.1088/0004-6256/140/1/184](https://doi.org/10.1088/0004-6256/140/1/184)
- Merle, T., Van der Swaelmen, M., Van Eck, S., et al. 2020, *Astronomy & Astrophysics*, 635, A155, doi: [10.1051/0004-6361/201935819](https://doi.org/10.1051/0004-6361/201935819)
- Milone, A. P., Piotto, G., Bedin, L. R., et al. 2012, *Astronomy & Astrophysics*, 540, A16, doi: [10.1051/0004-6361/201016384](https://doi.org/10.1051/0004-6361/201016384)
- Moe, M., & Di Stefano, R. 2017, *The Astrophysical Journal Supplement Series*, 230, 15, doi: [10.3847/1538-4365/aa6fb6](https://doi.org/10.3847/1538-4365/aa6fb6)
- Mugrauer, M., & Neuhauser, R. 2009, *A&A*, 494, 373, doi: [10.1051/0004-6361/200810639](https://doi.org/10.1051/0004-6361/200810639)
- NASA Exoplanet Archive. 2024, *Planetary Systems Composite Parameters*, Version: 2024-09-24 02:31, NExScI-Caltech/IPAC, doi: [10.26133/NEA13](https://doi.org/10.26133/NEA13)
- Naylor, T., & Jeffries, R. D. 2006, *Monthly Notices of the Royal Astronomical Society*, 373, 1251–1263, doi: [10.1111/j.1365-2966.2006.11099.x](https://doi.org/10.1111/j.1365-2966.2006.11099.x)
- Pearson, W. J., Wang, L., Trayford, J. W., Petrillo, C. E., & van der Tak, F. F. S. 2019, *A&A*, 626, A49, doi: [10.1051/0004-6361/201935355](https://doi.org/10.1051/0004-6361/201935355)
- Pietrzyński, G., Graczyk, D., Gieren, W., et al. 2013, *Nature*, 495, 76, doi: [10.1038/nature11878](https://doi.org/10.1038/nature11878)
- Price-Whelan, A. M., Hogg, D. W., Rix, H.-W., et al. 2018, *AJ*, 156, 18, doi: [10.3847/1538-3881/aac387](https://doi.org/10.3847/1538-3881/aac387)
- Pryor, C. P., Latham, D. W., & Hazen, M. L. 1988, *The Astronomical Journal*, 96, 123, doi: [10.1086/114795](https://doi.org/10.1086/114795)
- Qian, S.-B., Shi, X.-D., Zhu, L.-Y., et al. 2019, *Research in Astronomy and Astrophysics (RAA)*, 19, 64, doi: [10.1088/16744527/19/5/64](https://doi.org/10.1088/16744527/19/5/64)
- Raghavan, D., McAlister, H. A., Henry, T. J., et al. 2010, *The Astrophysical Journal Supplement Series*, 190, 1–42, doi: [10.1088/0067-0049/190/1/1](https://doi.org/10.1088/0067-0049/190/1/1)
- Sarro, L. M., Bouy, H., Berihuete, A., et al. 2014, *Astronomy & Astrophysics*, 563, A45, doi: [10.1051/0004-6361/201322413](https://doi.org/10.1051/0004-6361/201322413)
- Sheikhi, N., Hasheminia, M., Khalaj, P., et al. 2016, *Monthly Notices of the Royal Astronomical Society*, 457, 1028–1036, doi: [10.1093/mnras/stw059](https://doi.org/10.1093/mnras/stw059)
- Skrutskie, M. F., Cutri, R. M., Stiening, R., et al. 2006, *AJ*, 131, 1163, doi: [10.1086/498708](https://doi.org/10.1086/498708)
- Sollima, A., Carballo-Bello, J. A., Beccari, G., et al. 2010, *Monthly Notices of the Royal Astronomical Society*, 401, 577–585, doi: [10.1111/j.1365-2966.2009.15676.x](https://doi.org/10.1111/j.1365-2966.2009.15676.x)
- Srivastava, N., Hinton, G., Krizhevsky, A., Sutskever, I., & Salakhutdinov, R. 2014, *Journal of Machine Learning Research*, 15, 1929, <http://jmlr.org/papers/v15/srivastava14a.html>
- Steinmetz, M., Zwitter, T., Siebert, A., et al. 2006, *The Astronomical Journal*, 132, 1645–1668, doi: [10.1086/506564](https://doi.org/10.1086/506564)
- Tauris, T. M., & van den Heuvel, E. P. J. 2023, *Physics of Binary Star Evolution. From Stars to X-ray Binaries and Gravitational Wave Sources*, doi: [10.48550/arXiv.2305.09388](https://doi.org/10.48550/arXiv.2305.09388)
- Thebault, P., & Haghighipour, N. 2015, *Planet Formation in Binaries*, 309–340, doi: [10.1007/978-3-662-45052-9_13](https://doi.org/10.1007/978-3-662-45052-9_13)
- Ting, Y.-S., Hawkins, K., & Rix, H.-W. 2018, *ApJL*, 858, L7, doi: [10.3847/2041-8213/aabf8e](https://doi.org/10.3847/2041-8213/aabf8e)
- Torres, G., Andersen, J., & Giménez, A. 2010, *A&A Rv*, 18, 67, doi: [10.1007/s00159-009-0025-1](https://doi.org/10.1007/s00159-009-0025-1)

Traven, G., Feltzing, S., Merle, T., et al. 2020, A&A, 638, A145, doi: [10.1051/0004-6361/202037484](https://doi.org/10.1051/0004-6361/202037484)

Yan, L., & Mateo, M. 1994, The Astronomical Journal, 108, 1810, doi: [10.1086/117194](https://doi.org/10.1086/117194)

Zhang, B., Jing, Y.-J., Yang, F., et al. 2022, ApJS, 258, 26, doi: [10.3847/1538-4365/ac42d1](https://doi.org/10.3847/1538-4365/ac42d1)

Zhao, G., Zhao, Y.-H., Chu, Y.-Q., Jing, Y.-P., & Deng, L.-C. 2012, Research in Astronomy and Astrophysics, 12, 723, doi: [10.1088/1674-4527/12/7/002](https://doi.org/10.1088/1674-4527/12/7/002)